Ge-Aqueous-Electrolyte Interface: Electrical Properties and Electroreflectance at the Fundamental Direct Threshold

D. E. Aspnes

Bell Telephone Laboratories, Murray Hill, New Jersey 07974

and

A. Frova

Istituto di Fisica, Universita di Roma, Rome, Italy

(Received 20 October 1969)

Electroreflectance (ER) measurements at the $\Gamma_{8+} \rightarrow \Gamma_{7-}$ (fundamental direct) threshold are combined with electrical measurements in a detailed investigation of the nearly intrinsic Ge—neutral-aqueous-electrolyte interface. Capacitance and photovoltage (PV) measurements are combined to determine the flat-band potential and the impurity concentration of the space-charge region. These measurements show that no fast surface states are present for moderate modulating voltages for which the surface remains nondegenerate, and they allow the surface field to be calculated accurately over this range of surface potential. The instantaneous PV response shows that the Dember potential obeys quasiequilibrium equations for time intervals as short as 4 μsec. ER spectra are taken concurrently with measurements of the semiconductor surface field, yielding spectra suitable for quantitative interpretation. The very good agreement between these electrolyte and previously measured field-effect ER spectra indicates that the electrolyte ER spectra originate in the semiconductor, and demonstrates the equivalence of the two measurement techniques for this interface. By direct observation of the instantaneous reflectivity response, it is shown that surface states, generated electrochemically if intrinsic Ge is modulated beyond near-degeneracy ($\varphi_s \gtrsim 300$ mV), seriously influence observed ER spectra. The low-field measurements possible with the electrolyte technique indicate that the ER spectra do not vanish identically at flat band (zero surface potential and field) for symmetric modulation of intrinsic material, as expected, but rather reach a minimum for slightly p-type surfaces ($\varphi_s = 17$ mV, $\mathcal{E} \cong 260$ V/cm). The amplitudes of the observed ER spectra exceed the predictions of the Franz-Keldysh theory by over an order of magnitude at all fields, providing strong evidence of enhancement by the electron-hole Coulomb attraction and substantiating previous conclusions obtained primarily on the basis of line-shape arguments. It is shown that sufficient strength to produce the observed low-field ER spectra can come only from the $n = 1$ exciton absorption lines which lose their discrete nature at room temperature and behave as continuous states. The qualitative success of the inhomogeneous perturbation theory in describing line-shape evolution with increasing field appears to be due to the similarity of Franz-Keldysh and modulated continuum-exciton line shapes, together with a common dependence on the characteristic energy $\hbar\Omega$. A lifetime broadening of 1.8 ± 0.5 meV is deduced for this transition.

I. INTRODUCTION

The independent measurement of the electric field strength and its temporal and spatial dependence is essential in obtaining electroreflectance (ER) spectra suitable for quantitative interpretation, and particularly for line-shape analysis of symmetry and correlation effects.[1,2] It is generally recognized that transverse ER methods[3] and field-effect surface-barrier techniques[4] have been much more successful in obtaining quantitative ER spectra than electrolyte surface-barrier measurements,[5] in spite of several advantages which the latter method offers, such as intimate electrical contact to the semiconductor space-charge region (SCR) for direct capacitance measurement and surface-field determination, absolute calibration of ER spectra by eliminating effects of reflected light from dielectric layers, surface preparation by cleaning or electropolishing during measurement, and elimination of strain effects arising from contact of dissimilar solid materials at the semiconductor interface. Electrolyte ER has lagged behind the other methods principally because of electrochemistry problems, whose complexity usually prevents its advantages from being realized for many semiconductors. But even in the case of the Ge-aqueous-electrolyte system, which is relatively simple and well known,[6] electrochemical polarization effects cause slow changes to occur in the interface potential with corresponding drifts in effective operating points. These drifts

obscure and distort ER spectra, and necessitate continuous monitoring and adjustment of the electrolyte potential in order to obtain quantitative results.

Through the use of improved techniques, we have been able to perform the necessary simultaneous ER and surface-field measurements on the Ge-aqueous-electrolyte interface. It is the purpose of this paper to present quantitative electrolyte ER measurements of the $\Gamma_{8+} \rightarrow \Gamma_{7-}$ (fundamental direct) transition of Ge taken at this interface in order to demonstrate the equivalence between these and quantitative field-effect measurements,[7] and also to take advantage of the desirable properties of semiconductor-electrolyte systems to investigate more thoroughly the ER effect itself. In particular, we present spectra whose magnitudes far exceed those predicted by the simple Franz-Keldysh theory.[8] This effect suggests enhancement of these ER spectra by the electron-hole interaction,[9-11] substantiating previous conclusions based primarily on line-shape arguments.[12-15] Low-field measurements yield a broadening energy of 1.8 ± 0.5 meV for this transition, and also indicate that the ER spectra do not vanish at flat band for intrinsic Ge, as expected and usually assumed, but rather for the surface biased 17 ± 7 mV in the p-type (hole-accumulation) direction. Photovoltage (PV) measurements on this interface demonstrate that the Dember potential follows quasiequilibrium equations for time intervals at least as short as 4 μsec.

The outline of the paper is as follow: The experimental apparatus is discussed in Sec. II. Because improved techniques were needed to determine the surface field to the desired accuracy, we include their description as an electrical properties section, Sec. III, which is independent of the ER results presented and discussed in Sec. IV. Section III may be omitted if the ER results are of primary interest and if the error limits quoted in Sec. IV are accepted at face value. Over-all conclusions are presented in Sec. V.

II. EXPERIMENTAL

The block diagram of the apparatus is shown in Fig. 1 and is similar to systems previously described in the literature.[5,7] New features provide a means for measuring interface capacitance and PV, and also include a potentiostat system for control of the interface potential.

The optical system consisted of a Sylvania-type FCS tungsten-halogen light source, modulated at 30 Hz by a single-blade chopper with a duty cycle of 0.995. The source light was filtered by a Jarrell-Ash 1-m Czerny-Turner monochromator having a measured resolution of 1.0 meV in the wave-
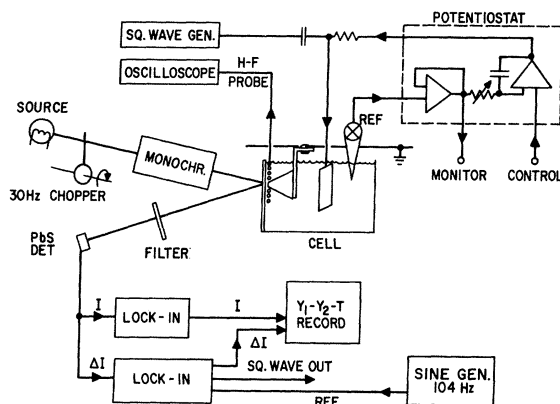

FIG. 1. Block diagram of the electronic and optical components of the measuring system.

length range of interest (1.5 to 1.7 μ). Wavelength calibration was performed using a low-pressure Hg arc lamp. Emerging light was directed onto the Ge sample, separated from the quartz cell window by about 0.5 mm of electrolyte. Only enough deviation from normal incidence was used to enable separation of the reflected from the incident beam. The reflected beam was focused through a Corning 7-56 IR-pass glass filter onto a 2×2-mm^2 Kodak Ektron PbS detector, which had a response time of 200 μsec. Not shown is an Electro-Nuclear Laboratories 1-mW HeNe laser, modulated by a phase-locked mechanical chopper with a switching time of 4 μsec. The laser illuminated the sample at normal incidence for PV measurements.

The electronic block diagram is also shown in Fig. 1. The reference frequency of 104 Hz for ER measurements was provided by a sine-wave oscillator. This supplied the reference channel of a Princeton Applied Research model HR-8 lock-in amplifier, which demodulated the signal proportional to the intensity change ΔI from the detector output. The 30-Hz signal, proportional to the total light intensity I and containing both window and sample contributions, was detected by a Princeton Applied Research Model 121 lock-in amplifier. The demodulated signals were simultaneously recorded on a y_1-y_2-t recorder. The intensity I was calibrated at a particular wavelength by scaling the recorded signal to the change in dc voltage observed at the PbS detector output (the oscilloscope in the "infinte" resistance mode[16]) with total chopping of the light beam. The window contribution to I was obtained at the end of each series of measurements by removing the sample and recording the resultant reflected intensity over the entire spectral range. This contribution, typically of the order of 20–40% of the total reflected in-

tensity, was subtracted from the recorded intensity before calculating $\Delta I/I = \Delta R/R$. The modulation signal ΔI was already calibrated, since the square-wave calibrator output of the HR-8 lock-in amplifier was used to provide the square-wave modulation voltage to the reference input of the potentiostat. Peak-to-peak values of ΔI were therefore obtained by multiplying the recorded signal by 2.22. Use of the calibrating waveform also provided a convenient check of phase shifts in the potentiostat and/or the ER response, and none were observed ($\pm 2°$). Resolution of $\Delta R/R$ was limited to about $\pm 2 \times 10^{-5}$ by rms noise of 200 nV.

The potentiostat controlled the electrolyte potential with respect to the grounded Ge working electrode. It consisted of a buffer operational amplifier and a driving operational amplifier with an RC feedback circuit.[17] The potentiostat acted as a high-impedance operational amplifier with variable response time, which held the electrolyte potential, as measured by a chemically isolated standard Calomel electrode, equal to an externally supplied dc-coupled reference voltage. Variable response time was necessary for stability and optimum waveform. The electrolyte potential was controlled by the output amplifier driving a platinum control electrode through a 10-$k\Omega$ resistor in order to provide a means of measuring sample current and interface capacitance.

The interface capacitance was measured by a high-frequency capacitive divider technique capable of making capacitance measurements within 1 μsec at any part of the modulation cycle. The method is described in detail elsewhere.[18] A 200-kHz square-wave generator connected through a 100-pF injection capacitor formed the source and known capacitance branch of the divider. The capacitance was obtained from the electrolyte potential response measured at a Pt high-frequency probe with the oscilloscope. The space-charge capacitance C_s was obtained by compensating for measured stray capacitances and the series capacitance of the Helmholtz region. Since the measured capacitance was always constant over each half of the square-wave modulation cycle after risetime transients, it was generally measured near the center of each half of the modulating cycle. The high-frequency probe was also used to monitor the fast PV response. The spacing between the sample and cell window was determined by observing the decay of the capacitive divider transient, and was set as small as possible without affecting the observed capacitance value obtained by extrapolating back from 1 μsec on the square-wave response. The electrolyte film thickness so determined was sufficient to provide enough conductivity

to assure reasonable uniformity of field over the surface of the Ge sample and adequate volume to allow removal of electrochemical reaction products by diffusion, while minimizing the optical path through the weakly absorbing electrolyte.[19]

The samples themselves were cut from two single crystals of Ge, one nominally intrinsic 40-Ω cm n-type Ge[20] and the other 49-Ω cm p-type Ge.[21] The samples were cut in the form of pyramids to decrease sample resistance, improve the Ohmic nature of the back contact by increasing its area, and increase the volume of electrolyte in the vicinity of the reflecting surface. Both (110) and (111) sample orientations were prepared for comparison purposes. The back face was approximately 1×1 cm^2 and the height 1 cm. Ohmic contacts were made by sandblasting and rhodium plating the back surface before soldering on the copper support. After mounting, the sides and apex of the pyramids were etched in CP-4 and the pyramid and supports were potted in Epoxy resin. After setting, the top of the pyramid was ground to an area roughly 2×3 mm^2 and optically polished, ending with 1-μ diamond paste. Two samples were electropolished with a KOH solution containing 0.05-μ alumina[22]; a third sample was given a Syton[23] polish for comparison purposes. All were electrochemically etched in the electrolyte for half an hour before making any ER measurements. After long periods in solution, the (111) surface developed etch pits, but the (110) surfaces remained flat, in accordance with the known morphology of these surfaces.[24]

The electrolyte was a 0.10M solution of K_2SO_4 in distilled water,[25] buffered with 0.025M Na_2HPO_4 and 0.025M KH_2PO_4 for a pH of 6.86.[26] The solution was cleaned by gettering with Ge crushed *in situ*. The electrolyte gave reproducible results and contained no impurities producing fast surface states, as shown by the capacitance and PV measurements.

III. ELECTRICAL PROPERTIES OF Ge-AQUEOUS-ELECTROLYTE INTERFACE

Since the interpretation of the ER results depends rather critically on a knowledge of the electrical properties of the interface, we discuss these in detail in this section. Of primary importance is the determination of sample doping in the SCR since the surface field calculated from the measured capacitance depends too strongly on this parameter to be able to use the nominal values. We outline a method of determining the sample doping, demonstrate its validity by several experimental cross checks, and compare measured interface parameters to theory. ER results are discussed in Sec. IV.

A. Potential Distribution and the Space-Charge Equations

The Ge—aqueous-electrolyte system has been extensively studies and much is known about its properties.[6] The flat-band or zero surface-field condition for nearly intrinsic Ge in a neutral solution occurs at about 200 to 300 mV anodic bias with respect to the standard Calomel electrode. This places the interface near the Ge-Ge(OH)$_2^{--}$ phase boundary,[27] and the resulting anodic current causes a continual slow dissolution of Ge from the crystal.[28] The products of the electrochemical reactions are water soluble, so no insulating layer is formed and a steady-state situation can be maintained. The I-V characteristics illustrated in Fig. 2 are typical of the interface, and were obtained from three samples used in ER measurements. The parameter λ in Fig. 2 indicates sample impurity concentrations, and is defined by

$$\lambda = n_B/n_i = n_i/p_B \quad , \tag{3.1}$$

where n_B and p_B are the bulk equilibrium electron and hole concentrations, and n_i is the intrinsic carrier concentration.

A dc steady-state bias divides between the semiconductor SCR and a surface dipole which depends on the bias condition, solution pH, and sample orientation and doping.[29-31] The flat-band position, indicated by an arrow in Fig. 2 for each sample, depends on surface orientation as well as sample doping.[24] The quiescent or open-circuit potential of the interface is unstable and depends on the amount of oxygen in solution.[32] It is evident that the surface dipole prevents the dc bias from being used as a measure of the semiconductor surface field. However, this dipole changes relatively slowly with time, so it is possible to apply rapid modulations (e.g., the 104-Hz potential used in this experiment) to vary the semiconductor potential.

The ac component of the total interface potential, caused by external electrolyte potential or illumination changes, can be divided into several parts of increasing order of importance. (a) There exists a potential drop in the electrolyte, the Gouy layer, or the SCR of the electrolyte, which can be completely neglected since the solute effectively provides a doping of 10^{22} cm^{-3} compared with a carrier concentration $n = p = n_i \cong 2.63 \times 10^{13}$ cm^{-3} for intrinsic Ge at 302 °K.[33] (b) There may be a Dewald potential,[34] which occurs for changes in illumination under constant-current bias. It is not relevant here since potentiostatic control is used and there are no constraints imposed on the current. (c) IR drops reach the millivolt range for currents of approximately 5 μA in our samples (100-μA/cm^2 current density). For large anodic bias, this causes the ac component in the
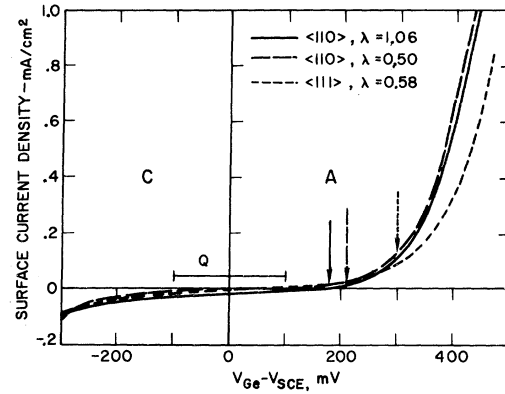

FIG. 2. Current-voltage characteristics of the three samples used in electrical and ER measurements. The potential of the Ge working electrode is measured with respect to the Calomel reference electrode. Q designates the observed range of the open-circuit interface potential. The location of the measured flat-band position for each crystal is indicated. The parameters λ refer to the measured doping of the crystals. A and C refer to anodic and cathodic bias, respectively.

surface potential φ_s to be less than the ac component of the total interface potential. It has no effect on the capacitance measurement from which the surface fields are determined. (d) A Dember potential occurs under illumination[35] since electrons are more mobile than holes. The Dember potential will be used to measure crystal doping and demonstrate the absence of surface states. It is given by

$$V_{Demb} = (kT/e)[(b-1)/(b+1)] \ln(\sigma_s/\sigma_b) \quad , \tag{3.2}$$

where σ_s, σ_b are the surface and bulk conductivities, respectively, and

$$\sigma_s = \sigma_b \left(1 + \alpha \frac{b+1}{1/\lambda + \lambda}\right), \tag{3.3}$$

with $b = \mu_n/\mu_p$ (mobility ratio)   (3.4a)

and $\alpha = \Delta n_s/n_i = \Delta p_s/n_i$ (injection ratio).   (3.4b)

$\Delta n_s = \Delta p_s$ is the nonequilibrium carrier concentration at the boundary between the quasineutral region and the SCR. Calculations indicate that the Dember potential is essentially instantaneous with respect to times of the order of microseconds.[36] The sign is such that the illuminated surface is more positive than the bulk. (e) The principal potential change appears across the SCR itself. Relations between the space-charge potential φ and the charge density ρ, electric field $\mathscr{E}$, total space charge Q_s, and space-charge capacitance C_s are given by the well-known equations[37,38]

$$\rho = -en_i\{\lambda e^y - (1/\lambda)e^{-y} - [\lambda - (1/\lambda)]\} \quad , \tag{3.5a}$$

$$\mathscr{E} = -\ \mathrm{sgn}(y)\ \mathscr{E}_{\mathrm{Db}}\left[\lambda(e^y - 1) + \frac{1}{\lambda}(e^{-y} - 1) - y\left(\lambda - \frac{1}{\lambda}\right)\right]^{1/2},$$
$$\tag{3.5b}$$

$$Q_s = \epsilon \mathscr{E}_s \ , \tag{3.5c}$$

$$C_s = -\rho_s / \mathscr{E}_s \ , \tag{3.5d}$$

where $\quad y = e\varphi/kT \tag{3.6}$

and the Debye field

$$\mathscr{E}_{\mathrm{Db}} = (2kTn_i/\epsilon)^{1/2} \ , \tag{3.7}$$

where ϵ is the static dielectric constant. The sign of the field corresponds to a semi-infinite solid filling $z \le z_s = 0$. The subscript s denotes a surface value. These equations are valid in the absence of surface states within the range of the Fermi level; we operate in a potential range where surface states are negligible.

Under illumination, it can be shown that the SCR in quasiequilibrium can be described exactly by substituting for n_i and λ in Eq. (3.4) the effective values

$$n_i' = n_i [1 + \alpha^2 + \alpha(\lambda + 1/\lambda)]^{1/2} \ , \tag{3.8a}$$

$$\lambda' = \left[\frac{\lambda + \alpha}{1/\lambda + \alpha}\right]^{1/2} . \tag{3.8b}$$

B. Determination of Sample Doping

In this section, we outline a combination of capacitance and PV measurements which will determine the sample doping, the flat-band or zero surface-field position ($\mathscr{E}_s = \varphi_s = 0$), and the concentration of excess carriers generated by uniform illumination. The method depends on measuring the difference between the value of φ_s, $\varphi_{s\,\mathrm{min}}$, at the space-charge capacitance minimum, $C_s = C_{\mathrm{min}}$, and the value of φ_s, φ_{s0}, at the zero of the fast PV response, i.e., the quantity $(\varphi_{s\,\mathrm{min}} - \varphi_{s0})$. Fast PV response is the "instantaneous" (less than 5 μsec) change in φ_s upon illumination of the crystal. $\varphi_{s\mathrm{min}}$ depends fairly strongly on the doping, whereas φ_{s0} is completely independent of doping. The reduced potential $y_{s\,\mathrm{min}}$ at $C_s = C_{\mathrm{min}}$ is obtained from Eq. (5). The values of λ which give $C = C_{\mathrm{min}}$ at $y = y_{s\,\mathrm{min}}$ are plotted in Fig. 3, together with the actual value of the capacitance at its minimum, for a range $|y_s| < 2.8$. The capacitance is given in units of the minimum value for intrinsic material,

$$C_0 = 2en_i/\mathscr{E}_{\mathrm{Db}} \ . \tag{3.9}$$

The almost complete independence of C_{min} on λ for $|y_{s\mathrm{min}}| < 1$, as shown in Fig. 3, suggests that the injection ratio α can be obtained from the ratio $C_{\mathrm{min}}'/C_{\mathrm{min}}$, where C_{min}' is the minimum value of the capacitance of an illuminated surface. By Eqs. (3.6), (3.8a), and (3.9), the square of this ratio gives directly
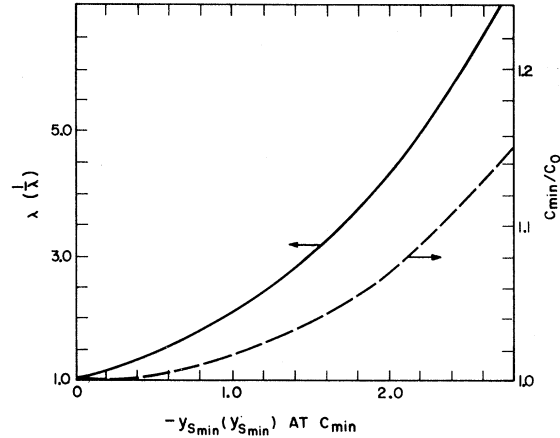

FIG. 3. Relation between $y_{s\mathrm{min}}$ and λ at the minimum value of space-charge capacitance C_{min}. The value of C_{min} in terms of the intrinsic minimum C_0 is also given.

$$(C_{\mathrm{min}}'/C_{\mathrm{min}})^2 = (C_0'/C_0)^2 [1 + \alpha^2 + \alpha(\lambda + 1/\lambda)]^{1/2} \ , \tag{3.10}$$

where the prefactor is a slowly varying function of λ by Fig. 3, and the prime refers to an illuminated surface.

The zero of PV can be found by calculating that value of y_s, or y_{s0}, for which a small change in illumination ($\alpha \to \alpha + \Delta\alpha$) results in no change in the semiconductor voltage, $\varphi_s + V_{\mathrm{Demb}}$, under the boundary condition of constant total space charge[39]:

$$\frac{\partial}{\partial\alpha}\left(\frac{kT}{e} y_s \Big|_{Q_s} + V_{\mathrm{Demb}}\right) = 0. \tag{3.11}$$

This is physically equivalent to requiring the illumination level change to occur in a time interval much shorter than the relaxation time for charge transfer across the interface. We find

$$y_{s0} = \ln b \ , \tag{3.12}$$

i.e., the zero of instantaneous photopotential for small changes in the injected carrier concentration depends only on the mobility ratio. For Ge at 302 °K, $\varphi_{s0} = 19$ mV and the zero of instantaneous PV occurs with the surface slightly n type with respect to flat band. It immediately follows that the difference between the values of φ_{s0} for initially illuminated and initially dark interfaces is just the Dember potential itself.

Interface parameters can now be determined by the following procedure. Flat band for $\varphi_s = 0$ is determined by measuring the zero of instantaneous PV and using Eq. (3.12). Sample doping is now obtained by measuring $\varphi_{s\,\mathrm{min}}$ at $C_s = C_{\mathrm{min}}$ and using

TABLE I. Comparison of theory and experiment for the determination of space-charge parameters by the method outlined in Sec. III B. The theory is cross checked by comparing the line pairs (3,4), (10,11), and (14,15), and by the capacitance ratio of line 7.

Line	Quantity	$\langle 110 \rangle 40 \ \Omega \ \mathrm{cm} \ N$	Crystal $\langle 110 \rangle 49 \ \Omega \ \mathrm{cm} \ P$	$\langle 111 \rangle 49 \ \Omega \ \mathrm{cm} P$
1	$\varphi_{s0} - \varphi_{s \ min}$ (expt)	21 ± 5 mV	-5 ± 5 mV	-1 ± 4 mV
2	$\varphi_{s min}$ (calc)	-2 ± 5 mV	24 ± 5 mV	20 ± 5 mV
3	λ (calc)	1.06 ± 0.1	0.5 ± 0.1	0.58 ± 0.1
4	λ (from ρ)	1.02 ± 0.1	0.7 ± 0.3	0.7 ± 0.3
5	area (expt)	0.071 cm^2	0.069 cm^2	0.110 cm^2
6	C_{min} (expt)	25.0 nF/cm^2	29.2 nF/cm^2	28.6 nF/cm^2
7	(% of theory)	118%	136%	133%
8	C'_{min} (expt)	37.7 nF/cm^2	43.0 nF/cm^2	35.0 nF/cm^2
9	α (calc)	1.12	1.16	0.35
10	V_{Demb} (calc)	6.5 mV	6.9 mV	2.8 mV
11	$\varphi'_{s0} - \varphi_{s0}$ (expt)	3 ± 1 mV	8 ± 1 mV	4.5 ± 1 mV
12	$\varphi'_{s0} - \varphi'_{s min}$ (expt)	21 ± 5 mV	10 ± 5 mV	6 ± 5 mV
13	$\varphi'_{s min}$ (calc)	-2 ± 5 mV	9 ± 5 mV	13 ± 5 mV
14	λ' (calc)	1.06 ± 0.1	0.77 ± 0.1	0.69 ± 0.1
15	λ'[from Eq. (3.8b)]	1.03	0.725	0.67

Fig. 3 to determine λ. After λ has been determined, the level of injection α follows from Eq. (3.10).

There are several other ways of obtaining the doping and flat-band bias which involve the use of PV, capacitance, or surface conductivity measurements, or combinations of the three. Surface conductivity is difficult to measure at an electrolyte interface. The doping can be obtained in principle by measuring the saturation values of the PV for large cathodic and anodic bias,[37] but this method requires invariance of Q_s which is usually not realized over millisecond periods. For these and other reasons, more accurate values of space-charge parameters can be obtained from the procedure outlined here.

C. Results and Discussion

Table I summarizes the results of the above procedure when applied to the samples used for ER measurements. The results are reproducible to within the given error limits. Primed quantities refer to an illuminated interface. Line 1 is used to calculate $\varphi_{s min}$, which is given in line 2, by using $\varphi_{s0} = 19$ mV from Eq. (3.12). λ given in line 3 follows immediately from Fig. 3. This value should be compared with that calculated from the nominal resistivity of the p-type samples and given in line 4.[40] The experimental values of C_{min} per unit area, shown in line 6 and expressed as a percentage of their theoretical values in line 7, provide another comparison of theory and experiment. The experimental values of C'_{min} given in line 8, together with line 6 and Eq. (3.12), enable α to be calculated as shown in line 9. Given α and λ, the Dember potential is calculated from Eq. (3.2) and

shown in line 10. It can be compared with the difference between the experimental values of φ_{s0} starting from illuminated and dark steady-state conditions, respectively, given in line 11. Finally, λ may be determined directly from φ'_{s0} and $\varphi'_{s min}$ by the same procedure if n'_i and λ', defined by Eqs. (3.8), are used in place of n_i and λ, since the theory is invariant with respect to this substitution. Starting with line 12 and using $\varphi'_{s0} = 19$ mV, $\varphi'_{s min}$ is calculated in line 13, from which λ' follows in line 14 by Fig. 3. A final comparison of theory and experiment is possible by calculating λ' from Eq. (3.8b) using lines 3 and 9. The results of this calculation are given in line 15.

Table I gives four cross checks which support the theory and show in addition that surface states are absent, and that the quasiequilibrium equations apply to both φ_s and the Dember potential. These checks occur for the values of λ given in lines 3 and 4, the capacitance percentage of line 7, the Dember potentials of lines 10 and 11, and the effective dopings under illumination given by lines 14 and 15. The agreement between all values of λ and λ' for the intrinsic crystal is excellent. The value of λ obtained by capacitance and PV measurements agrees with that obtained from the nominal resistivity for the p-type material, but the uncertainty is considerably less. The agreement between the Dember potentials of lines 10 and 11 specifically indicates a lack of surface states, for surface states would strongly affect the SCR contribution to the total PV but would leave the Dember contribution essentially unchanged, and the measured and calculated Dember voltages would differ (additional evidence of the absence of surface states
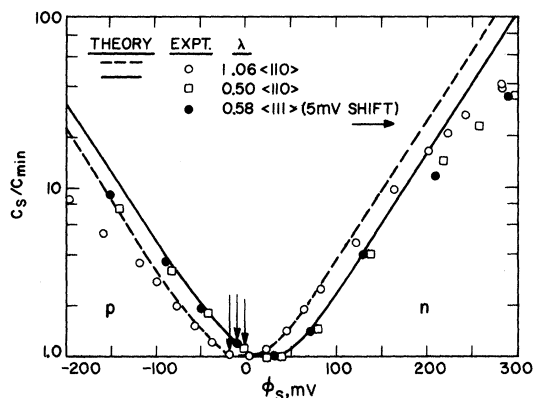
FIG. 4. Comparison of the theoretical and measured space-charge capacitance C_s for each crystal. The experimental points were taken during a series of ER measurements. The arrows show the reference potential for the modulating voltage. For clarity, the $\lambda = 0.58$ theoretical curve has been omitted and the corresponding experimental points have been shifted 5 mV to coincide with the $\lambda = 0.50$ theoretical curve.

is found in the measured capacitance-voltage characteristics[41] shown later). The excellent agreement between the two experimentally determined values of λ given in rows 3 and 4 for the intrinsic sample can only occur if in addition the Dember potential can be described as a quasiequilibrium process with respect to the 4-μsec risetime of the light pulse. If this assumption were incorrect, the value of λ in row 3 would be 0.6 larger due to the 19-mV shift in φ_s. The measured minimum capacitance is expected to be of the order of 25% larger than the theoretical value, as shown in row 7, principally because of surface roughness[42] and edge effects. The excellent agreement between the values of λ' in lines 14 and 15 provides further substantiation of the theory and results.

Two points should be mentioned. First, the capacitance and PV measurements are necessarily averages over the entire surface and therefore determine average parameters. Uniformity must be demonstrated in order to show that average and local values are equal. To do this, we have measured the PV response to a highly focused beam scanned over the surface, and have found the local zero PV response always occurs within 2 mV of the average value φ_{s0}. Some deviation occurred at the extreme edges at the Ge-Epoxy bond, but these edge effects are negligible when averaged over the entire surface. Since φ_{s0} is a fixed potential, the flat-band conditions deviated less than 2 mV across the entire surface of each crystal studied. Second, all potential differences have been measured with a 104-Hz square wave. This is essential, for sur-

face dipole relaxation in dc measurements leads to (observed) increases of about a factor of 2 in all potential differences in Table I for a {110} surface (less for the more stable {111} surfaces), even if the measurements are taken within 10 sec of each other. This leads to the failure of all cross checks discussed in connection with Table I.

A comparison of the measured capacitance with its theoretical variation is shown in Fig. 4. These data were taken simultaneously with measurements of ER spectra to be given later. The experimental points are plotted versus the applied modulating square-wave voltage V_s, which is referenced to zero at the values of φ_s for which the ER signal reached a minimum for each sample (and indicated by arrows in Fig. 4). Theory and data for the $\lambda = 0.58$ crystal are shifted 5 mV to simplify display. The excellent agreement for $|\varphi_s| < 100$ mV illustrates that fast surface states have negligible effect,[41] and that no overvoltage is appearing across the Helmholtz region[29,30] in this potential range. Deviation occurs for large cathodic bias because of voltage drops across the Helmholtz region, and for large anodic bias because of resistive losses in the sample (see Fig. 2). The capacitance, however, remains a true measure of φ_s.[29,30]

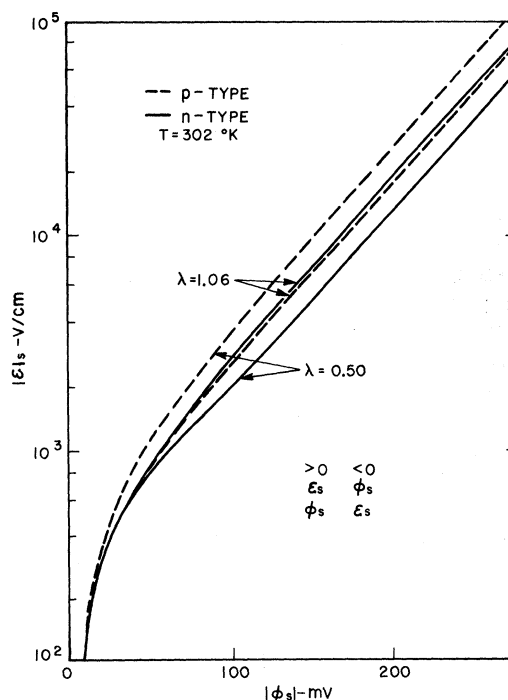The surface field can now be obtained accurately from the measured capacitance and the values of

FIG. 5. Theoretical relation between surface field $\mathcal{E}_s$ and surface potential φ_s for the crystals used in the experiment.

λ given in Table I. The surface field $\mathcal{E}_s$ as a function of φ_s is given in Fig. 5, where φ_s is determined from C_s by Fig. 4. $\mathcal{E}_s$ is most accurately determined for $|\varphi_s| < 100$ mV, where the ± 5 and ± 2 mV uncertainties in φ_s arising from uncertainties in determining λ and C_s, respectively, lead to an error of ± 100 V/cm or 10% in $\mathcal{E}_s$, whichever is greater. For large bias ($|\varphi_s| > 150$ mV), accuracy was reduced because the relaxation time for charge transfer across the interface became comparable to the relaxation time of the capacitance-measuring voltage pulse. For large cathodic bias ($\varphi_s > 300$ mV, surface strongly n type), surface-state formation was observed, appearing as an increase in C_{min} of at least a factor of 2.[30] These states could be removed by anodic etching. No ER spectra were taken when the surface was influenced by these states. Finally, minor changes of the order of 10% in the value of C_{min} would occur over a series of ER measurements and were completely explained by the temperature dependence of n_i.[33] C_{min} was always measured between ER spectra in order to provide proper normalization for measured values of C_s and therefore eliminate errors in obtaining φ_s from Fig. 4.

IV. ER RESPONSE OF Ge-AQUEOUS-ELECTROLYTE INTERFACE

A. Origin of Electrolyte ER Spectra

Reflectivity modulation of semiconductor-electrolyte interfaces can be produced or otherwise influenced by chemical reactions as well as changes in the semiconductor SCR. Before discussing the ER spectra in detail, we show that they are not modified by chemical effects over the range of modulating potentials used here. This is done (a) by demonstrating that the electrolyte ER spectra are in very good agreement with those obtained by field-effect measurements,[7] and (b) by using sufficiently large modulating potentials so that chemical effects may be seen explicitly.

A typical example of the agreement generally found between quantitative field effect[7] and the electrolyte ER spectra to be presented here is shown in Fig. 6. Several electrolyte ER spectra taken on three different samples are shown together with one field-effect spectrum in order to illustrate in addition the general reproducibility of our results, and their independence on sample preparation and orientation. The results shown in Fig. 6 provide evidence that these spectra originate from changes in the semiconductor rather than from chemical reactions, in that the electrolyte spectra agree very well not only with the field-effect measurements but also with *each other* for different surface orientations. We emphasize that the electrolyte ER results of Fig. 6 are quantitative; the ex-
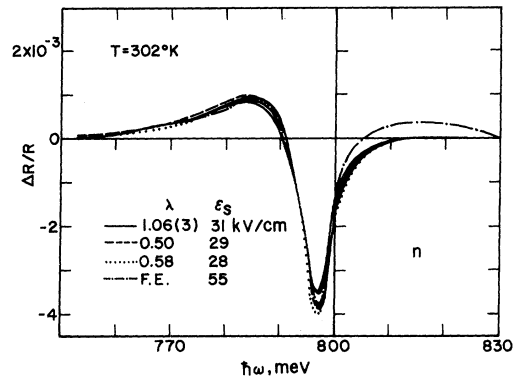

FIG. 6. ER spectra for the three samples of Table I taken at 300-mV modulation with cathodic bias (flat-band to n-type modulation). Also shown is a normalized curve taken from the field-effect results of Ref. 7.

perimental electrolyte spectra have not been scaled (the dry sandwich spectrum was multiplied by 1.51 to bring the main negative peak into coincidence with the electrolyte results; it appears smaller in the original spectrum due to reflection from the Mylar film and SnO_2 contact of the field-effect sandwich). The 10% reproducibility is typical of these electrolyte spectra, and the 10% limitation exceeds any dependence of the spectra upon sample orientation and preparation, following an anodic etch of 1 mA/cm² for a few minutes after initial preparation. The smaller values quoted for the surface field $\mathcal{E}_s$ of the electrolyte spectra are due partly to systematic errors in the capacitance measurement for large fields (> 15 kV/cm) and are discussed in Sec. III.

Further evidence of the semiconductor origin of electrolyte ER spectra at low modulation potentials can be obtained by comparing the instantaneous reflectivity change $\Delta R(t)/R$ to the modulating potential $V_s(t)$ [not the SCR surface potential $\varphi_s (t)$] for moderate and excessivly large modulation. At excessive modulation levels, effects due to the electrochemistry of the interface can be seen explicitly. Figure 7 illustrates this comparison in both cases. Figures 7(b) and 7(d) represent $\Delta R(t)/R$ measured at the ER peak at $\hbar\omega = 799.2$ meV, using a Princeton Applied Research Model TDH-9 waveform eductor. Figures 7(a) and 7(c) show the time variation of the electrolyte or modulating potential which produce the spectra below. Figures 7(a) and 7(b) represent a moderate square-wave modulation of 190 mV (flat band to hole accumulation). The ER response of Fig. 7(b) follows the modulating voltage to at least the detector response time of 200 μsec, consistent with the known SCR response time of less than 1 μsec as observed in capacitance[18,42] and electroabsorption[43] measurements. The droop
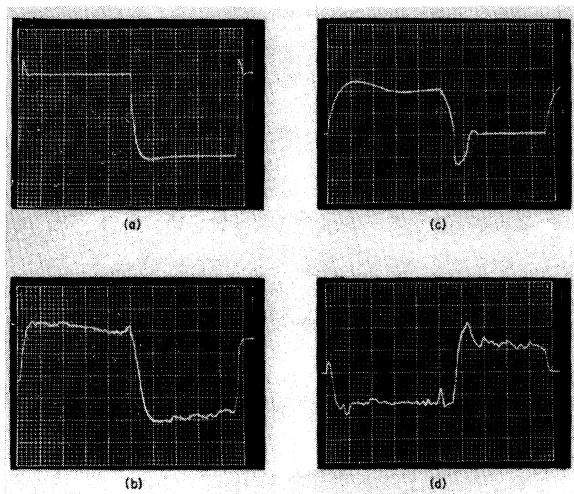
FIG. 7. Real-time ER response of the interface for
p-type (left) and excessive n-type (right) modulations.
The upper curves show the electrolyte potentials for the
ER responses below. All measurements were taken at
$\hbar\omega = 799.2$ meV, from flat band to the bias shown. The
horizontal time scales are 1 msec/(large division)
(104-Hz modulation frequency). The vertical scales
are upper left: 50 mV/(large division); lower left:
10 μV/(large division); upper right: 200 mV/(large di-
vision); lower right: 25 μV/(large division). The dc
light intensity for these measurements (including window
contribution) was 34 mV.

in the flat portions of $\Delta R(t)/R$ is due entirely to
low-frequency rolloff in the preamplifier.

Chemical effects due to excessive modulating
voltages can be seen explicitly in Fig. 7(d), which
gives the instantaneous response $\Delta R(t)/R$ for 400-
mV square-wave modulation of Fig. 7(c) (flat band
to electron accumulation). Figures 7(b) and 7(d)
exhibit the typical inversion which occurs in ER
spectra as the surface polarity is reversed.[31,44]
The excessive modulating voltage electrochemical-
ly generates surface states, causing the severe
distortion of the electrolyte voltage in Fig. 7(c) at
the end of the positive (electron accumulation) half
of the modulation cycle. These states prevent $\mathcal{E}_s$
from returning to zero until they are etched away
by the negative voltage overshoot. Figure 7(d)
shows that $\Delta R(t)/R$ does not return to its reference
value for 600 μsec, or until surface-state removal
is completed. Surface-state generation is also in-
dicated directly by large increases in the minimum
value of the space-charge capacitance at these mod-
ulation levels. We note that even if the chemical
reactions occurring at excessive modulating
voltages do not change the reflectivity directly as,
for example, by synchronously generating a highly
absorbing film, it is evident that Ge—electrolyte
ER spectra can be used for quantitative interpreta-

tion only as long as the modulating voltage does
not drive the surface to degeneracy in intrinsic
material. The much larger modulation voltages
used in all previously reported electrolyte ER ex-
periments have almost certainly influenced the re-
sulting ER spectra through these effects.

B. Reference Reflectivity

Of fundamental importance in the measurement
of $\Delta R/R$, particularly at low modulation levels, is
the determination of that value of surface potential
$\varphi_s = \varphi_{s0}$ for which $R = R_0$, i.e., the reflectivity is
that of the unperturbed surface. Then by definition

$$\Delta R/R = (R - R_0)/R_0 \ . \qquad (4.1)$$

All uniform field theories[8-11] predict an even de-
pendence of $\Delta R/R$ on $\mathcal{E}_s$. Therefore, φ_s can be
determined in principle by measuring the average
or dc value of φ_s, $\bar{\varphi}_s$, at which $\Delta R/R$ vanishes for
any symmetric modulating waveform. It is usually
assumed that the value $\bar{\varphi}_s = \varphi_{s0}$ so determined is
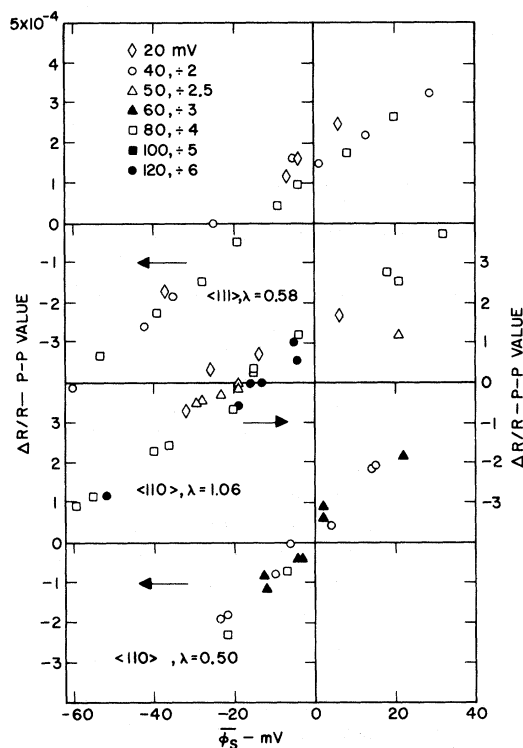zero (flat band). Although this is not strictly true

FIG. 8. Peak-to-peak ER response for fixed mod-
ulation amplitude and varying dc bias for each crystal
of Table I. These measurements define the zero
ER response. Data points representing the different
modulation levels are scaled as indicated in the upper
left corner. φ_s is the average space-charge region
potential for each modulating signal. "$\div n$" means that
the values have been divided by n before plotting.

in an extrinsic semiconductor due to different ac-
cumulation and depletion field profiles, it should
be identically true in an intrinsic crystal. Sur-
prisingly, we have found that $\Delta R/R$ does *not* van-
ish identically for intrinsic Ge at any value of φ_s,
and that the minimum value of $\Delta R/R$ does not even
occur at flat band, but for $\varphi_s = (-17 \pm 7)$ mV, cor-
responding to a slightly p-type surface with a sur-
face-field strength of about $\mathcal{E}_s \cong 260 \pm 100$ V/cm.

Measurements which lead to this conclusion are
presented in Fig. 8. Because $\Delta R/R$ does not van-
ish, we define "vanishing" as the extrapolation to
zero of the peak-to-peak value of $\Delta R/R$ for *fixed*
modulation voltage amplitude and variable dc bias,
with the sign of $\Delta R/R$ being that of the average sur-
face potential $\overline{\varphi}_s$. The data in Fig. 8 are identified
by the amplitude of the square-wave modulation,
and are all normalized to 20-mV modulation by
linear scaling as shown in the upper corner. $\Delta R/R$
vanishes at $\overline{\varphi}_s = -3$ mV, -17 mV, and -15 mV in
the $\langle 110 \rangle \lambda = 0.50$, the nearly intrinsic $\langle 110 \rangle \lambda = 1.06$,
and the $\langle 111 \rangle \lambda = 0.58$ crystals, respectively. These
values are observed to be independent of the mod-
ulating voltage amplitude V_s, at least to 120 mV,
and are reproducible to within 2 mV from day to
day.

Since this in some sense defines a minimum or
extremum value of R, we define R_0 and φ_{s0} to cor-
respond to the value of $\overline{\varphi}_s$ at which $\Delta R/R$ vanishes
for symmetric modulation, even though the crystal
is not quite in the zero-field or flat-band condition.
These are the potentials indicated by arrows in
Fig. 4. This choice does not noticeably affect
spectral line shapes, since the high-field half of
the modulation cycle completely dominates for mod-
ulation levels in excess of 100 mV, and the line
shapes are nearly independent of field below this
level as will be shown. Since $\mathcal{E}_s$ is nonzero at
R_0, the reference reflectivity, surface-field values
quoted for specific spectra will be differences mea-
sured with respect to this value. The success of
the linear scaling procedure in Fig. 8 indicates
that ER spectra for low modulation levels are bi-
linear in $(\overline{\varphi}_s - \varphi_{s0})$ and ΔV, where ΔV is the am-
plitude of the modulation. From Fig. 8,

$$\Delta R/R \big|_{p-p} = (0.43 \pm 0.10)\,\Delta V(\overline{\varphi}_s - \varphi_{s0})\,V^{-2} . \quad (4.2)$$

This form shows that the nonzero value of φ_{s0} can
be interpreted phenomenologically in terms of a
weak second ER mechanism roughly linear in φ_s.
The origin of this linear effect is obscure; the two
obvious linear effects, free-carrier absorption and
electrochemically generated films, are estimated
to produce $\Delta R/R$ signals of the order of 10^{-9} and
10^{-8}, both much too small to be observed. In ad-
dition, they should have a broad spectral response
whereas the lack of zero offset in the experimental

spectra implies that the linear term is connected
with the main structure of the $\Delta R/R$ signal. Low-
level field-effect ER measurements should indicate
whether this is an effect in the crystal or an arti-
fact associated with the electrolyte techniques. A
possible explanation may lie in the field inhomoge-
neity acting on the exciton envelope, in view of the
large difference between electron and hole effec-
tive masses. The observed bilinearity of $\Delta R/R$
predicts that the line shape of $\Delta R/R$ obtained by
lock-in detection is independent of the line shape
of the modulating potential for all waveforms to
the extent that the entire spectrum scales as the
peak-to-peak value, since the bilinear form does
not mix harmonics in the modulating voltage.

C. ER Spectra and Discussion

A complete set of ER spectra for the nearly in-
trinsic crystal is shown in Figs. 9 and 10. The
data are divided into a low-field region given in
Fig. 9 and distinguished by virtually no dependence
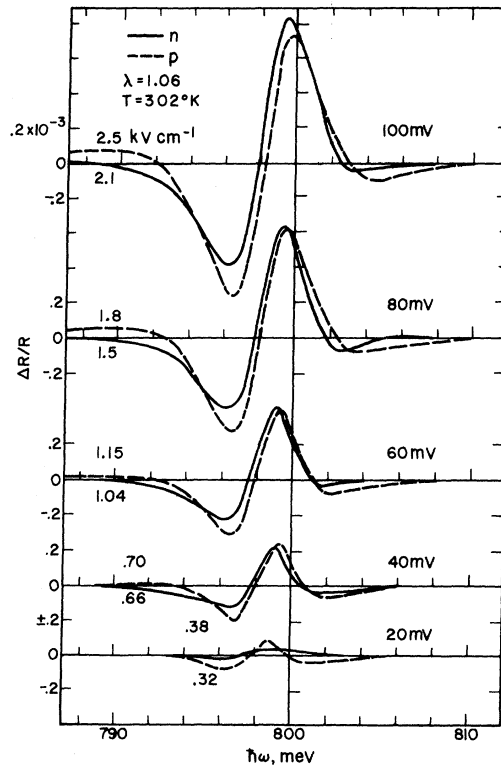of the spectral line shape on $\mathcal{E}_s$, and a high-field

FIG. 9. Evolution of the ER spectra of the nearly in-
trinsic sample through the low-field range, character-
ized by invariance of line shape to modulating field. The
magnitudes of the modulating voltages are shown on the
right for each pair of curves; the corresponding values
of the difference between maximum and zero-ER surface
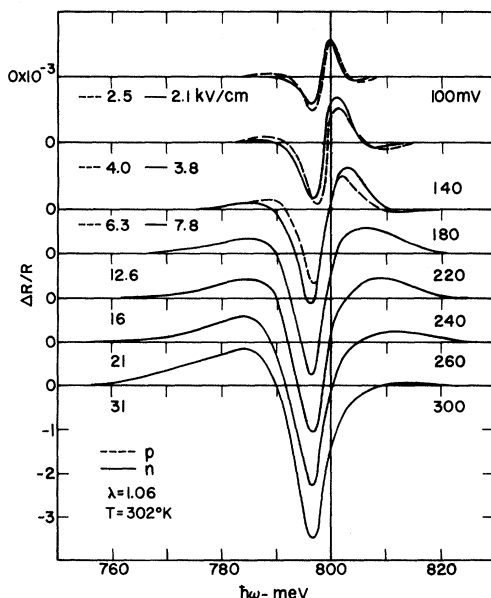fields for each curve are shown on the left.

FIG. 10. Evolution of the ER spectra for the sample of Fig. 9 through the high-field region. The amplitude of the square-wave modulation voltage is shown on the right and the corresponding surface-field difference on the left.

region given in Fig. 10, where the spectra broaden and undergo considerable change with increasing field. The square-wave modulating voltages appear on the right. The values of $\mathscr{E}_s$ on the left are calculated from the space-charge capacitance as discussed in Sec. III. Only spectra taken on the $\lambda = 1.06 \langle 110 \rangle$ Ge sample are shown, since all samples gave similar results. Figure 10 shows data taken to the maximum modulation levels attainable with this interface. Anodic modulation (p-type surface) was current limited; resistivity drops in the crystal and electrolyte at the 140- and 180-mV modulation levels are apparent because both $\mathscr{E}_s$ and the amplitude of $\Delta R/R$ are lower for anodic than cathodic bias for these modulations. Cathodic modulation was limited by the formation of surface states. The capacitance data plotted in Fig. 4 were obtained concurrently with these measurements.

The curves of Fig. 9 present data taken at lower modulation levels than previously reported. The fairly simple spectral line shape remains invariant, scaling quadratically with modulating voltage as described phenomenologically by Eq. (4.2)(note that the dc bias must vary half as fast as the modulation amplitude). Certain systematic differences between cathodic and anodic polarizations are apparent at the ends of the spectra in that the anodic bias response overshoots at the low-energy end,

whereas the cathodic bias response overshoots at the high-energy end. This is further evidence of a small component in the ER spectra which has a different functional dependence on potential than the dominant part. The spectrum corresponding to the larger surface field of any pair is always larger except at the lowest modulation, where the experimental errors were of the order of the uncertainties in $\Delta R/R$ and $\mathscr{E}_s$.

In principle, the line shapes of Figs. 9 and 10 could be calculated from the general theory which combines Coulomb and uniform electric field effects,[9-11] but this theory has not been developed in a form readily suited for lifetime broadening and direct experimental comparison. Approximate limiting forms are adequate for our interpretation, and in some cases provide better insight into the physical processes involved. The relation between the local field-induced change in the dielectric function $\Delta \epsilon(z)$ and the observed spectra $\Delta R/R$ for nonuniform fields is given by

$$\Delta R/R \cong 0.0109(\langle \Delta \epsilon_1 \rangle + 0.04 \langle \Delta \epsilon_2 \rangle) , \quad (4.3)$$

where[7,45]

$$\langle \Delta \epsilon \rangle = \langle \Delta \epsilon_1 \rangle + i \langle \Delta \epsilon_2 \rangle$$

$$= -2iKe^{2iKz_s} \int_{-\infty}^{z_s} dz' e^{-2iKz'} \Delta \epsilon(z') \quad (4.4)$$

and $(cK/\omega)^2 = \epsilon$.

The coefficients[46] in Eq. (4.3) were evaluated for a Ge–aqueous-electrolyte interface at $z = z_s$ ($n_{Ge} = 4.1$, $\alpha_{Ge} \cong 3500$ cm^{-1} at $\hbar\omega = 0.80$ eV,[47,48] $n_{water} = 1.33$). Since the propagation vector $\vec{K}$ is nearly real, $\Delta R/R$ is approximately proportional to $\Delta \epsilon_1(z_s)$ in the uniform field limit.

We consider first the spectra in the low-field limit given by Fig. 9, where the line shapes are determined by the combination of broadening inherent in the sample together with the measured 1.0-meV resolution of the monochromator. The small dependence of $\mathscr{E}$ on z in intrinsic Ge increases the coefficient of $\langle \Delta \epsilon_2 \rangle$ from 0.04 to 0.13 in Eq. (4.3). This is small enough to be safely neglected; we will discuss Fig. 9 in the uniform field approximation and use only the first term in Eq. (4.3). Three physical mechanisms which could lead to these line shapes will be investigated: $n = 1$ exciton line broadening, continuum exciton broadening, and the Franz-Keldysh effect.

The spectra of Fig. 9 can in principle arise from a shift or broadening of the $n = 1$ exciton absorption line; the shift mechanism was used by Lange and Gutsche to describe electroabsorption in CdS.[49] The dielectric function for this line is given by the expression[50]

$$\epsilon(\omega) = -\frac{Q_0}{\omega^2}\frac{8\pi}{r_0^3}\frac{1}{\omega - (\omega_g - \omega_{ex}) + i\Gamma} \quad , \qquad (4.5)$$

where $\quad r_0 = \dfrac{\kappa_0 m_e}{\mu} a_B = 25.6$ nm, heavy hole

$\qquad\qquad\qquad = 43.3$ nm, light hole

$$\hbar\omega_{ex} = \frac{\mu}{\kappa_0^2 m_e}E_{Ry} = 1.04 \text{ meV, light hole}$$

$$= 1.73 \text{ meV, heavy hole}$$

$$Q_0/\omega^2 = (4\pi^2 e^2 |\hat{e}\cdot\vec{P}_{cv}|^2/m^2\omega^2\hbar)\, 2/(2\pi)^3$$

$$\cong 3.1\times10^{-13} \text{ m}^3\text{sec}^{-1} \text{ at } \hbar\omega = 0.800 \text{ eV} \quad ,$$

r_0 is the exciton radius, $\hbar\omega_{ex}$ is the binding energy, $\vec{P}_{cv}$ is the momentum matrix element, $\hbar\Gamma$ is the broadening energy, and $\hbar\omega_g$ is the critical-point threshold. r_0 and $\hbar\omega_{ex}$ were calculated from the values $\kappa_0 = 16$ for the dielectric constant, and $0.0195m_e$ and $0.0325m_e$ for the room-temperature light- and heavy-hole reduced masses, respectively.[51] The quantity Q_0/ω^2 was evaluated at $\hbar\omega = 800$ meV using the value $|\hat{e}\cdot\vec{P}_{cv}| = 0.37\hbar/a_B$ calculated from the limit of continuum absorption ($\alpha = 3500$ cm^{-1}) observed at room temperature[47] ($\vec{k}\cdot\vec{P}$ theory[52] and the integrated absorption under the $n = 1$ absorption line for the strain-split heavy-hole exciton in Vrehen's data[53] yield $0.39\hbar/a_B$ and $0.36\hbar/a_B$, respectively, for the momentum matrix element, in good agreement with the absorption measurements).

The respective line shapes arising from field-induced changes in either ω_{ex} or Γ are readily calculated from Eq. (4.4), and only the line shape for field-dependent broadening agrees with the spectra of Fig. 9. Thus, field-induced broadening should dominate any field-induced shift in $\hbar\omega_{ex}$. This is in agreement with the predictions of the general theory,[9-11] and consistent with results discussed later. Since the quantitative variation of $\hbar\Gamma_{ex}$ on $\mathcal{E}$ is not available in a form suited for computation, we will estimate only the maximum possible contribution from the $n = 1$ exciton absorption line, which is just equal to the contribution to R from the line itself. It is easily shown from Eqs. (4.3) and (4.5) that the peak-to-peak amplitude of the line in R is $R_{ex} = 1.8\times10^{-3}$, including both light- and heavy-hole excitons.[54] This number was calculated using $\hbar\Gamma = 2.2$ meV, obtained by noting (a) the observed peak separation on the energy axis is 2.5 ± 0.3 meV and (b) for low fields, we should observe not ϵ_1, but rather $\partial\epsilon_1/\partial\Gamma$, which has similar form but whose peaks are separated by an energy $2\hbar\Gamma/\sqrt{3}$.[49] Correcting for the 1.0-meV monochromator resolution would lead to an actual broadening of 1.3 ± 0.3 meV on the basis of this mechanism.

It is evident that the $n = 1$ exciton structure possesses sufficient strength to cause the observed low-field structure. Yet further considerations

indicate that the model is oversimplified — it is expected that the contributions from the light- and heavy-hole excitons should saturate for fields of the order of their respective ionizing fields, $\epsilon\mathcal{E}_i r_0 = \hbar\omega_{ex}$, or 240 V cm^{-1} and 675 V cm^{-1}. This saturation has been observed explicitly at 77 °K by Vrehen in electroabsorption on a sample with strain-split excitons.[53] However, Fig. 9 shows no such saturation tendency at these field levels. Second, absorption measurements[47,48] show that the $n = 1$ exciton line is mixed into continuum states at room temperature where $\hbar\Gamma$ is of the order of the binding energy. This suggests that the continuum contribution must also be considered as a source of these spectra.

Modulation of the continuum absorption, which includes the Coulomb interaction, is a second possible mechanism. The dielectric function of the zero-field continuum exciton is described by[55]

$$\epsilon_2(\omega) = (Q_0/\omega^2)\,(2\mu/\hbar)\,(4\pi^2/r_0)$$

$$\times\{1 - \exp[-2\pi\,(\hbar/2\mu r_0^2(\omega - \omega_g))^{1/2}]\}^{-1} \quad . \tag{4.6}$$

The expression is approximated to within 30% for $\hbar|\omega - \omega_g| < 10$ meV, the range of interest in Fig. 9, by neglecting the exponential term. In this limit, and in the limit of large broadening, it can be shown that the convolution integral describing electric field effects on ϵ_2 reduces to the simple asymptotic expression[56]

$$\Delta\mathcal{E}(\omega, \Gamma, \mathcal{E}) \sim -\frac{2}{3}\frac{Q_0}{\omega^2}\left(\frac{2\mu}{\hbar}\right)\times\frac{4\pi}{r_0}\frac{\Omega^3}{(\omega - \omega_g + i\Gamma)^3} \quad , \tag{4.7}$$

where $\quad \hbar\Omega = (e^2\mathcal{E}^2\hbar^2/8\mu)^{1/3} \quad . \tag{4.8}$

Rees[57] has shown that the convolution integral formalism has approximate validity in the continuum, and this is substantiated by the observed field dependence of subsidiary oscillations in both electroabsorption[12] (EA) and low-temperature ER[14] data. Equation (4.7) is applicable so long as the characteristic energy $\hbar\Omega$ is less than $\hbar\Gamma$, or $\mathcal{E}_s \lesssim 1000$ V/cm. Below this value, the theoretical curve simply scales quadratically in field, as is observed in Fig. 9. The line shape $\Delta\epsilon_1$ given by Eq. (4.7) is virtually identical to those in Fig. 9 but the calculated magnitude is too small by a factor of 5. For instance, using previously determined values and a field strength of 1000 V/cm, $\hbar\Omega$ is 1.70 and 1.43 meV for light and heavy holes, respectively. The energy separation between the main peaks of $\Delta\epsilon_1$ from Eq. (4.7) is $0.830\hbar\Gamma$, giving $\hbar\Gamma = 3.0$ meV, which yields a total contribution to $\Delta R/R$ of 1.6×10^{-4} compared to the observed value of 7×10^{-4} at this field, and the maximum possible contribution estimated to be 18×10^{-4} from the $n = 1$ exciton lines.

The third possible mechanism is the Franz-Keldysh effect, which would occur if the Coulomb interaction were absent. The exact broadened expression[58]

$$\Delta \mathscr{E}(\omega, \Gamma, \mathscr{E}) = (Q_0/\omega^2)\,(2\mu/\hbar)^{3/2}\theta^{1/2}$$

$$\times \{2\pi[e^{i\pi/3}\mathrm{Ai}(z)\,\mathrm{Ai}(w) + w\mathrm{Ai}(z)\,\mathrm{Ai}(w)] + \sqrt{z}\} \,, \tag{4.9}$$

where $z = (\omega_g - \omega - i\Gamma)/\theta$, $w = ze^{2\pi i/3}$;

$$\theta^3 = 4\Omega^3$$

has the limiting form[56]

$$\Delta\epsilon(\omega, \Gamma, \mathscr{E}) \sim \frac{i\pi}{4}\frac{Q_0}{\omega^2}\left(\frac{2\mu}{\hbar}\right)^{3/2}\Omega^3(\omega - \omega_g + i\Gamma)^{-5/2} \,, \tag{4.10}$$

whose real part $\Delta\epsilon_1$ again has a line shape similar to those in Fig. 9. But using the fact that the energy separation of the main peaks is $1.026\hbar\Gamma$, we find the total contribution to $\Delta R/R$ from both light- and heavy-hole bands to be 0.16×10^{-4}, compared with 1.6×10^{-4} for the Coulomb continuum, 7×10^{-4} observed experimentally, and an upper limit of 18×10^{-4} available from the $n = 1$ exciton lines.

The above figures show that completely neglecting the Coulomb interaction leads to a theoretical ER spectrum which is small by a factor of 45. This clearly indicates that the Coulomb interaction must be included in the theoretical description of the low-field structure and substantiates previous conclusions based primarily on line-shape arguments.[12,14] Second, the continuum contribution, even in the presence of the Coulomb interaction, is too small by a factor of 5 to account for the observed spectra. This suggests that the major contribution to the ER spectra must come from the $n = 1$ exciton lines, but the observed lack of saturation indicates that these lines have become mixed with the continuum at room temperature, completely losing their discrete identity.

We now examine the high-field data given in Fig. 10, which show the evolution of the spectral line shape for increasing modulation levels. These spectra are in very good agreement with the field-effect data given in Fig. 6 of Ref. 7. The main features of the spectra, the saturation of the main negative peak with increasing field and the increase and decrease in the lower-energy (red) and higher-energy (blue) positive peaks, respectively, are qualitatively accounted for by the theory of inhomogeneous perturbations as discussed more fully in Refs. 7 and 45. Rather than repeat the detailed comparison of peak-height and peak-energy separation versus field for each of the three main peaks in the line shape of Fig. 10, as done in Figs. 11 and 12 of Ref. 7, we mention that these results are substantially unchanged except that the lower
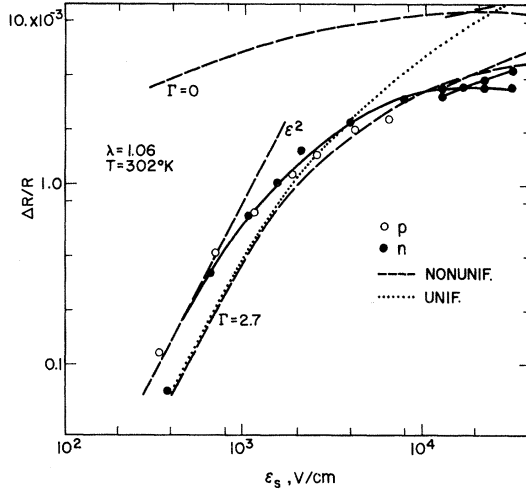

FIG. 11. Variation of the peak-to-peak value of $\Delta R/R$ for the results of Figs. 9 and 10. The theoretical curves are scaled by adjusting the value of the momentum matrix element as described in the text. Above the cross-over field of 16 kV/cm, the peak-to-peak value of $\Delta R/R$ is determined by the lower-energy positive peak.

measured field for the electrolyte curves improves agreement in the energy position (Fig. 12 of Ref. 7) and reduces the agreement in the relative peak height (Fig. 11 of Ref. 7). The crossover field, defined as that value of $\mathscr{E}_s$ where the red and blue positive peaks have equal magnitude, occurs at 16 kV/cm in the electrolyte and 30 kV/cm in the dry sandwich results. The inhomogeneous perturbation theory based on the one-electron approximation predicts 18 kV/cm for $\hbar\Gamma = 2.7$ meV, in reasonable agreement.

As a means of comparing magnitudes, we plot the peak-to-peak value of $\Delta R/R$ as a function of field against the inhomogeneous perturbation theory in Fig. 11. The experimental data are taken from Fig. 9 and 10. For fields less than 16 kV/cm, this difference is taken between the main negative and the blue positive peak. For higher fields, the red positive peak is used. Above 10 kV/cm, both experimental values are given, illustrating the crossover. The theoretical curves are calculated from the Franz-Keldysh theory given by Eq. (4.9) for both $\hbar\Gamma = 0$ and $\hbar\Gamma = 2.7$ meV, where the spatial dependence of the field is taken to be that of intrinsic Ge. For comparison, one curve for $\hbar\Gamma = 2.7$ meV was calculated in the uniform field approximation. All theoretical curves include both light- and heavy-hole contributions, and all have the same relative normalization which is given by a momentum matrix element $|\hat{\epsilon}\cdot\vec{P}_{cv}|$ $= 1.36\hbar/a_B$.

The low-field square-law behavior clearly requires broadening to be included in the theory. In order to obtain the experimentally observed peak saturation and crossover, the broadening must be supplemented by the spatial broadening of the inhomogeneous perturbation, as is evident in Fig. 11. If both lifetime and inhomogeneous perturbation broadening are included in the theory, the high-field experimental data are apparently quite well described in the Franz-Keldysh approximation. Transverse ER measurements on semi-insulating GaAs also show qualitative agreement with this theory, without inhomogeneous broadening.[59]

Yet as with the low-field data, the Franz-Keldysh theory fails to account for the observed magnitude of $\Delta R/R$. One comparison can be made between the saturation value of the main negative peak in Fig. 10 and that predicted by theory. Since both theory and experiment yield a saturation, it is expected that these numbers can be reliably compared regardless of uncertainties in the actual value of $\mathcal{E}_s$. The experimental saturation value of $\Delta R/R = -(3.6 \pm 0.3) \times 10^{-3}$ is obtained either from Fig. 10 or Fig. 6. For the momentum matrix element $|\hat{e} \cdot \vec{P}_{cv}| = 0.37 \hbar/a_B$ theory predicts a saturation value $\Delta R/R = -0.24 \times 10^{-3}$, 15 times smaller. This is confirmed by Fig. 11; the matrix element of $1.36 \hbar/a_B$ required for proper normalization multiplies the theoretical curves by a factor of $(1.36/0.37)^2 = 13.5$. This appears to be in agreement with recent measurements of Handler, Jasperson, and Koeppen,[60] who observed the subsidiary oscillations predicted by the Franz-Keldysh theory at higher fields for this threshold, and who find them to be much smaller than the main structure would suggest. As with the low-field data, it appears necessary to include Coulomb interaction enhancement to describe the high-field data in the vicinity of the critical point, again in qualitative agreement with exact theories.[9-11] The observed spreading of the line shape with increasing field provides additional evidence that the $n = 1$ exciton lines have effectively replaced their discrete nature with continuum behavior, otherwise a fixed-width remnant of the relatively strong totally ionized discrete lines should be observable in the high-field spectra.

From Figs. 9–11 and the associated discussion, we draw the following conclusions. (1) The Coulomb interaction strongly influences ER at the fundamental direct edge in Ge. This follows from calculations which show that quantitative experimental ER spectra are more than an order of magnitude too large at all fields to arise from a simple Franz-Keldysh effect, but are consistent with magnitudes calculated from simple models which include the Coulomb interaction. This is in agreement with previous conclusions based on line-shape arguments.[12,14] (2) Inhomogeneous perturbation effects determine the line shape at high fields in intrinsic Ge. No other mechanism can account for the observed crossover in amplitude of low- and high-energy positive peaks seen in Fig. 10. It appears that the good agreement between the broadened Franz-Keldysh based theoretical curve and experiment in Fig. 11 is due mainly to the similarity in line shapes between broadened Franz-Keldysh and exact theories, and the fact that both utilize the same characteristic energy $\hbar\Omega$ at high fields. (3) Only the $n = 1$ exciton lines possess sufficient oscillator strength to account for the observed magnitudes of the low-field spectra, but the spreading and growth of these spectra with increasing field is indicative of a continuum origin. Therefore, at room temperature, the $n = 1$ exciton states appear to act as continuum states. This is consistent with the observed lifetime broadening and exciton binding energies for this transition. (4) The broadening energy for this transition lies somewhere between 1.3 meV ($n = 1$ exciton line prediction) and 2.0 meV (continuum exciton prediction). Most likely, the higher value is correct; we take the broadening as $\hbar\Gamma = 1.8 \pm 0.5$ meV, in good agreement with the value of 3 meV obtained by Handler et al.[60] which was not corrected for monochromator resolution.

Finally, it is of interest to compare our results with those of Hamakawa et al.,[13] who also quoted surface fields for specific ER spectra. The comparison cannot be made directly, since they used dc interface control and sine-wave modulation of amplitude up to 1.4 V, both of which cause other effects which influence $\Delta R/R$. Nevertheless, their comparative field technique enables their ER spectra to be used as a bridge to their previously measured electroabsorption data,[12] where the fields were well determined by capacitance measurements on thin reverse-biased diodes or on thin intrinsic Ge samples with evaporated Au contacts. The important feature is the appearance of a crossover in the heights of the low- and high-energy positive peaks in the K-K transform of the EA spectra, indicating that inhomogeneous perturbations are also important in EA.[47] Their value of the surface field at which crossover occurs (19 kV/cm) is in excellent agreement with ours, and lends further support to this conclusion.

V. CONCLUSION

In this paper, the intrinsic Ge–aqueous-electrolyte system has been investigated in detail regarding electrical properties and ER spectra of the

fundamental direct threshold. In Sec. III, a procedure for obtaining the impurity concentration in the surface region, necessary for calculating the surface field from the capacitance, was developed and experimentally verified. The Dember potential was shown to obey quasiequilibrium equations over microsecond intervals. The results of these measurements enabled the Ge surface potential φ_s to be determined within 7 mV for $|\varphi_s| < 100$ mV, including uncertainties in the doping in the surface region. The results demonstrated that dc measurements of the space-charge potential are inaccurate, and that quantitative measurement of any space-charge-dependent quantity, such as ER, requires simultaneous measurement of the surface field.

The ER results presented in Sec. IV showed that the quantitative field-effect and electrolyte data were in very good agreement. In addition, it was shown that the time response of ER was consistent with that observed in EA,[43] except when excessive modulation voltages caused additional effects to occur due to surface states. These observations prove that ER spectra obtained by the electrolyte technique originate from modulation of the Ge SCR, and not to chemical effects. Since the surface potential was well determined, the correlation between flat-band potential and the bias for which the ER response vanished for symmetric modulation was investigated, and it was found that the minimum $\Delta R/R$ response occurred for a surface biased about 17 ± 7 meV p type with an intrinsic sample. Since in addition the ER response failed to vanish identically at any bias potential for symmetric modulation, the presence of a small additional component in ER, not described by existing theoretical approximations, is indicated. The

narrow spectral range of this component demonstrates its connection with the dominant ER mechanism, but its origin is obscure and further work is needed to clarify its cause.

The evolution of the ER line shape with increasing field shows that the inhomogeneous perturbation average must be included in the qualitative description, in agreement with the field-effect measurements.[7] Both low- and high-field measurements show the Coulomb interaction strongly influences on the line shape, since the Franz-Keldysh theory underestimates observed spectra by more than an order of magnitude. Therefore, we have confirmed on quantitative grounds similar conclusions previously reached primarily on line-shape arguments.[12,14] Quantitative estimates also indicate that the predominant ER contribution arises from the $n = 1$ exciton line, but that this line behaves as the continuum at room temperature due to thermal mixing. It appears that the very good agreement between the experimental results and the predictions of the inhomogeneous perturbation theory[47] must come at least in part from a strong line-shape similarity between Franz-Keldysh and exciton continuum modulated line shapes (in particular, a common dependence on the same characteristic energy $\hbar\Omega$), coupled with the inhomogeneity itself exerting the dominant line-shape-determining influence. A broadening energy of 1.8 ± 0.5 meV is deduced for this transition.

ACKNOWLEDGMENTS

[1]M. Cardona, *Modulation Spectroscopy* (Academic, New York, 1969).

[2]B. O. Seraphin, in *Semiconductors and Semimetals*, edited by R. K. Willardson and A. C. Beer (Academic, New York, 1966), Vol. 8.

[3]C. Gahwiller, Helv. Phys. Acta **39**, 595 (1966); Solid State Commun. **5**, 65 (1967); V. Rehn and D. Kyser, Phys. Rev. Letters **18**, 848 (1967); R. A. Forman and M. Cardona, in *Physics of Semiconductors, Providence*, edited by D. G. Thomas (Wiley, New York, 1968), p. 100.

[4]B. O. Seraphin, in *Proceedings of the Seventh International Conference on the Physics of Semiconductors, Paris*, 1964 (Academic, New York, 1964), p. 165; B. O. Seraphin and R. B. Hess, Phys. Rev. Letters **14**, 138 (1965); B. O. Seraphin and N. Bottka, *ibid.* **15**, 104 (1965); A. Frova and P. J. Boddy, Phys. Rev. **153**, 606 (1967).

[5]K. L. Shaklee, F. H.' Pollak, and M. Cardona,

Phys. Rev. Letters **15**, 883 (1965); K. L. Shaklee, M. Cardona, and F. H. Pollak, *ibid.* **16**, 48 (1966); M. Cardona, K. L. Shaklee, and F. H. Pollak, Phys. Rev. **154**, 696 (1967).

[6]A comprehensive account of the work on this interface can be found in V. A. Myamlin and Yu. V. Pleskov, *Electrochemistry of Semiconductors* (Plenum, New York, 1967).

[7]A. Frova and D. E. Aspnes, Phys. Rev. **182**, 795 (1969).

[8]D. E. Aspnes and N. Bottka, in Ref. 2.

[9]H. I. Ralph, J. Phys. C **1**, 378 (1968).

[10]D. F. Blossey, Ph. D. thesis, University of Illinois, 1969 (unpublished); P. Handler and D. F. Blossey, in Ref. 2.

[11]J. D. Dow and D. Redfield, Phys. Rev. D **1**, 3358 (1970).

[12]Y. Hamakawa, F. A. Germano, and P. Handler, Phys. Rev. **167**, 703 (1968); J. Phys. Soc. Japan Suppl.

21, 111 (1966).

[13]Y. Hamakawa, P. Handler, and F. A. Germano, Phys. Rev. 167, 709 (1968).

[14]Y. Hamakawa, T. Nishino, and J. Yamaguchi, in *Proceedings of the Ninth International Conference on the Physics of Semiconductors*, edited by S. M. Ryvkin (Nauka Publishing House, Leningrad, 1968), p. 384.

[15]T. Nishino and Y. Hamakawa, J. Phys. Soc. Japan 26, 403 (1969).

[16]A Tektronix type 547 oscilloscope with type W preamplifier was used for all measurements in this paper.

[17]Type 148B FET operational amplifiers, manufactured by Analog Devices, Inc., Cambridge, Mass.

[18]D. E. Aspnes, J. Electrochem. Soc. 116, 585 (1969).

[19]It has been brought to our attention that D_2O is nearly transparent in this wavelength region, as compared to H_2O which was used in this experiment.

[20]Obtained from Eagle-Picher Co., Quapaw, Okla.

[21]Obtained from Western Electric Corp., Allentown, Pa.

[22]T. M. Donovan and B. O. Seraphin, J. Electrochem. Soc. 109, 877 (1962).

[23]Manufactured by Monsanto Chemical Co., St. Peters, Mo.

[24]P. J. Boddy, J. Electrochem. Soc. 111, 1136 (1964).

[25]W. H. Brattain and P. J. Boddy, J. Electrochem. Soc. 109, 574 (1962).

[26]*Handbook of Chemistry and Physics*, 45th ed. (Chemical Rubber Co., Cleveland, 1964), p. D-72.

[27]M. Pourbaix, *Atlas D' Equilibres Electrochimiques* (Gauthier-Villars, Paris, 1963), p. 464ff. Note that at 302 °K, the temperature of all measurements performed in this experiment, the hydrogen electrode is 0.655 V more negative than the Calomel reference electrode at a pH of 6.86.

[28]W. H. Brattain and C. G. B. Garrett, Phys. Rev. 94, 750 (1954); F. Beck and H. Gerischer, Z. Elektrochem. 63, 500 (1959); Ref. 6, pp. 193–197.

[29]H. Gerischer, A. Maurer, and W. Mindt, Surface Sci. 4, 431 (1966); H. Gerischer, M. Hoffman-Perez, and W. Mindt, Ber. Bunsenges Physik. Chem. 69, 130 (1965).

[30]H. Gobrecht, R. Thull, F. Hein, and M. Schaldach, Ber. Bunsenges. Physik. Chem. 73, 68 (1969).

[31]B. O. Seraphin, Surface Sci. 13, 136 (1969).

[32]W. W. Harvey and H. C. Gatos, J. Electrochem. Soc. 107, 65 (1960).

[33]R. A. Smith, *Semiconductors* (Cambridge U. P., Cambridge, England, 1961), p. 359.

[34]J. F. Dewald, in *Surface Chemistry of Metals and Semiconductors*, edited by H. C. Gatos (Wiley, New York, 1960), pp. 205–224.

[35]W. van Roosbroeck, Phys. Rev. 91, 282 (1953); Ref. 6, p. 109.

[36]A complete solution of the diffusion and space-charge equations as a function of time would be required to sat-

isfactorily demonstrate this. We will show experimental verification.

[37]C. G. B. Garrett and W. H. Brattain, Phys. Rev. 99, 376 (1955).

[38]R. H. Kingston and S. F. Neustadter, J. Appl. Phys. 26, 718 (1955).

[39]W. Mindt and H. Gerischer, Surface Sci. 9, 449 (1968).

[40]The value for the nearly intrinsic 40-Ω cm sample was accurately determined for an adjacent part of the original boule from the measured resistivity maximum of 2100 Ω cm at about 200 °K, together with a low-temperature Hall measurement which showed n-type conduction.

[41]W. H. Brattain and P. J. Boddy, *Physics of Semiconductors, Exeter* (Cambridge U. P., Cambridge, England, 1962), p. 797.

[42]P. J. Boddy and W. Sundburg, J. Electrochem. Soc. 110, 1170 (1963).

[43]A. Frova and P. Handler, Phys. Rev. 137, A1857 (1965); Y. Yacoby, *ibid*. 142, 445 (1965).

[44]B. O. Seraphin, R. B. Hess, and N. Bottka, J. Appl. Phys. 36, 2242 (1965).

[45]D. E. Aspnes and A. Frova, Solid State Commun. 7, 155 (1969).

[46]B. O. Seraphin and N. Bottka, Phys. Rev. 145, 628 (1966).

[47]G. G. Macfairlane, T. P. McLean, J. E. Quarrington, and V. Roberts, Proc. Phys. Soc. (London) 71, 863 (1958).

[48]W. C. Dash and R. Newman, Phys. Rev. 99, 1151 (1955).

[49]H. Lange and E. Gutsche, Phys. Status Solidi 32, 293 (1969).

[50]R. J. Elliott, Phys. Rev. 108, 1384 (1957); S. Nikitine, *Progress in Semiconductors* (Wiley, New York, 1962), Vol. 6, pp. 233ff.

[51]S. Zwerdling, B. Lax, and L. M. Roth, Phys. Rev. 108, 1402 (1957); R. N. Dexter, H. Y. Zeiger, and B. Lax, *ibid*. 104, 637 (1956).

[52]E. O. Kane, J. Phys. Chem. Solids 1, 243 (1957).

[53]Q. H. F. Vrehen, Phys. Rev. 145, 675 (1966).

[54]We neglect degeneracy effects. This has been shown a reasonable approximation in the presence of an electric field by R. Enderlein, R. Keiper, and W. Tausenfreund, Phys. Status Solidi 33, 69 (1969).

[55]L. D. Landau and E. M. Lifshitz, *Quantum Mechanics* (Pergamon, Oxford, 1965), pp. 116–122.

[56]D. E. Aspnes and J. E. Rowe, Solid State Commun. (to be published).

[57]H. D. Rees, J. Phys. Chem. Solids 29, 143 (1968); Solid State Commun. 5, 365 (1967).

[58]D. E. Aspnes, Phys. Rev. 153, 972 (1967).

[59]R. A. Forman, D. E. Aspnes, and M. Cardona, J. Phys. Chem. Solids 31, 227 (1970).

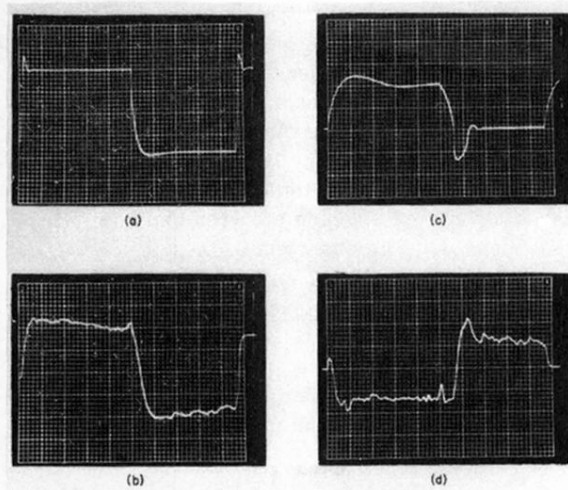[60]P. Handler, S. Jasperson, and S. Koeppen, Phys. Rev. Letters 23, 1387 (1969).

FIG. 7. Real-time ER response of the interface for p-type (left) and excessive n-type (right) modulations. The upper curves show the electrolyte potentials for the ER responses below. All measurements were taken at $\hbar\omega = 799.2$ meV, from flat band to the bias shown. The horizontal time scales are 1 msec/(large division) (104-Hz modulation frequency). The vertical scales are upper left: 50 mV/(large division); lower left: 10 μV/(large division); upper right: 200 mV/(large division); lower right: 25 μV/(large division). The dc light intensity for these measurements (including window contribution) was 34 mV.